Inorganic Chemistry
Article

Inorg. Chem. **2010**, *49*, 1921–1931 **1921**
DOI: 10.1021/ic902343r

X-Ray Diffraction and μ-Raman Investigation of the Monoclinic-Orthorhombic Phase Transition in $Th_{1-x}U_x(C_2O_4)_2 \cdot 2H_2O$ Solid Solutions

Nicolas Clavier,*[,†,‡] Nina Hingant,[‡] Murielle Rivenet,[§] Saïd Obbade,[§] Nicolas Dacheux,[†,‡] Nicole Barré,[‡] and Francis Abraham[§]

[†]*ICSM—UMR 5257 CNRS/CEA/UM2/ENCSM, Centre de Marcoule, Bât. 426, BP 17171, 30207 Bagnols/Cèze, France,* [‡]*Groupe de Radiochimie, IPNO—UMR 8608 CNRS/UPS-11, Bât. 100, Univ. Paris-Sud-11, 91406 Orsay, France, and* [§]*UCCS—UMR 8181, ENSCL, Cité Scientifique—Bât. C7, BP 90108, 59652 Villeneuve d'Ascq cedex, France*

Received November 26, 2009

A complete $Th_{1-x}U_x(C_2O_4)_2 \cdot 2H_2O$ solid solution was prepared by mild hydrothermal synthesis from a mixture of hydrochloric solutions containing cations and oxalic acid. The crystal structure has been solved from twinned single crystals for x=0, 0.5, and 1 with monoclinic symmetry, space group *C*2/*c*, leading to unit cell parameters of $a \approx 10.5$ Å, $b \approx 8.5$ Å, and $c \approx 9.6$ Å. The crystal structure consists of a two-dimensional arrangement of actinide centers connected through bis-bidentate oxalate ions forming squares. The actinide metal is coordinated by eight oxygen atoms from four oxalate entities and two water oxygen atoms forming a bicapped square antiprism. The connection between the layers is assumed by hydrogen bonds between the water molecules and the oxygen of oxalate of an adjacent layer. Under these conditions, the unit cell contains two independent oxalate ions. From high-temperature μ-Raman and X-ray diffraction studies, the compounds were found to undergo a transition to an orthorhombic form (space group *Ccca*). The major differences in the structural arrangement concern the symmetry of uranium, which decreases from *C*2 to *D*2, leading to a unique oxalate group. Consequently, the ν_s(C−O) double band observed in the Raman spectra recorded at room temperature turned into a singlet. This transformation was then used to make the phase transition temperature more precise as a function of the uranium content of the sample.

Introduction

Several actinide-based materials, including oxides, carbides, or nitrides, are currently studied as potential fuels for the fourth generation (Gen-IV) of nuclear reactors.[1] Among them, actinide mixed dioxides are already successfully employed in pressurized water reactors and are envisaged in several Gen-IV concepts such as sodium-cooled fast reactors[2] or very high-temperature reactors.[3] The extreme environment associated with these reactors (temperature, pressure, radiation)[4] as well as the necessity to develop a sustainable fuel cycle require control of the physicochemical properties of the fuel material on the micro-, meso-, and even nanometric scales.

Currently, mixed actinide dioxide fuels (such as UO_2/PuO_2) are prepared through dry chemistry routes based on powder mixtures. Nevertheless, it could result in some heterogeneity in the distribution of the cations in the structure.[5] Since wet chemistry methods generally provide more homogeneous samples than dry chemistry routes, the preparation of the $Th_{1-x}U_xO_2$ model compounds was undertaken through precipitation processes leading to crystallized precursors,[6] as a model for the forthcoming synthesis of $Th_{1-x}Pu_xO_2$, $Th_{1-x}Np_xO_2$, or $U_{1-x}Pu_xO_2$ compounds. The final goal of this study aims to correlate the nature of the precursor and its method of preparation to the microstructure of the final dioxide and some interesting properties such as the chemical durability. Indeed, some recent studies already demonstrated that the preparation method could significantly influence the behavior of actinide dioxides during dissolution[7−9] and sintering processes.[10]

*To whom correspondence should be addressed. Tel: +33 4 66 33 92 08. Fax: +33 4 66 79 76 11. E-mail: nicolas.clavier@icsm.fr.

(1) *A Technology Roadmap for Generation IV Nuclear Energy Systems* (http://www.gen-4.org/PDFs/GenIVRoadmap.pdf, accessed Jan 2010), issued by D.O.E and Generation IV Forum, **2002**.
(2) Ichimiya, M.; Sagayama, Y. T. *Am. Nucl. Soc.* **2004**, *90*, 46–47.
(3) Hoffelner, W. *Chimia* **2005**, *59*, 977–982.
(4) Oudinet, G.; Munoz-Viallard, I.; Aufore, L.; Gotta, M. J.; Becker, J. M.; Chiarelli, G.; Castelli, R. *J. Nucl. Mater.* **2008**, *375*, 86–94.
(5) Buisson, P. Ph.D. Thesis, University Grenoble 1, Grenoble, France, GRE1-0519, **1999**.
(6) Arab-Chapelet, B.; Grandjean, S.; Nowogrocki, G.; Abraham, F. *J. All. Compds.* **2007**, *444*/*445*, 387–390.
(7) Heisbourg, G.; Hubert, S.; Dacheux, N.; Ritt, J. *J. Nucl. Mater.* **2003**, *321*, 141–151.
(8) Heisbourg, G.; Hubert, S.; Dacheux, N.; Purans, J. *J. Nucl. Mater.* **2004**, *335*, 5–13.
(9) Hingant, N.; Clavier, N.; Dacheux, N.; Barré, N.; Hubert, S.; Obbade, S.; Taborda, F.; Abraham, F. *J. Nucl. Mater.* **2009**, *385*, 400–406.
(10) Hingant, N.; Clavier, N.; Dacheux, N.; Hubert, S.; Barré, N.; Podor, R.; Aranda, L. *Powder Tech.* **2010**, in press.

Published on Web 01/22/2010

Several compounds are usually reported in the literature as precursors for the preparation of actinide dioxides, including carbonates,[11] nitrates,[12] or hydroxides.[13] Among them, oxalate compounds are probably the most frequently employed due to the good properties exhibited by the final solids obtained after heating at high temperatures, particularly concerning the sintering capability[14] and the grain size homogeneity.[15] Also, it was recently evidenced that the use of hydrothermal conditions during the synthesis could lead to the preparation of original compounds, usually unreachable through conventional methods, such as the orthorhombic $U(C_2O_4)_2 \cdot 2H_2O$[16] and the monoclinic $Th(C_2O_4)_2(H_2O)_2 \cdot 2H_2O$.[17] These phases also generally exhibit the properties described above in terms of sintering capability and homogeneity.[18]

Numerous papers described the crystal structure of various actinide-bearing oxalates, the nature of the lattice being mostly dependent on the oxidation state of the cation. The chemistry of uranyl oxalates appears to be very rich since at least a dozen different structures were refined due to the various combinations in the $UO_2^{2+}/C_2O_4^{2-}$ ratio and in the nature of the monovalent cation incorporated.[19−21] For mixed An^{IV}/Ln^{III}[22−24] or An^{IV}/An^{III}[25] compounds, three different structures are reported, depending mainly on the An(IV)/An(III) nature and the An(IV)/An(III) ratio. Among them, the hexagonal $M_{2+x}An^{IV}_{2-x}An^{III}_x(C_2O_4)_5 \cdot nH_2O$ and the tetragonal $M_{1-x}[An^{III}_{1-x}An^{IV}_x(C_2O_4)_2 \cdot H_2O] \cdot nH_2O$ (where M is a single-charged cation incorporated to ensure the electroneutrality) solid solutions were of particular interest since they allow the coconversion of tri- and tetravalent actinides into mixed fluorite-type oxides after heat treatment at high temperatures. Finally, the crystal structure of tetravalent actinide oxalates mainly varies with the hydration of the samples. Indeed, a triclinic structure was reported in the mid 1960s for $An^{IV}(C_2O_4)_2 \cdot 6H_2O$ (An^{IV} = Th, U, Np, Pu) from powdered compounds by Bressat et al.[26] and Jenkins et al.[27] before it was assumed to be a monoclinic lattice from the data collected on neptunium-based single crystals as reported by Grigor'ev et al.[28] For dihydrated $An^{IV}(C_2O_4)_2 \cdot 2H_2O$ (An^{IV} = Th, U) compounds, an orthorhombic lattice is generally assumed.[16,27] On this basis, the preparation of oxalate precursors of $Th_{1-x}U_xO_2$ ($0 \le x \le 1$) solid solutions from hydrothermal conditions was undertaken in this work. The formation of a complete solid solution $Th_{1-x}U_x(C_2O_4)_2 \cdot 2H_2O$ was carefully investigated through X-ray diffraction, and it was revealed that the actual symmetry of the dihydrate is monoclinic. A transition to the orthorhombic form was evidenced by high-temperature X-ray diffraction and μ-Raman studies, and this is discussed on the basis of the crystal structure of both forms (monoclinic and orthorhombic), determined from single crystals at room temperature and 90 °C, respectively. Moreover, the influence of the amount of uranium on the μ-Raman spectrum of both crystalline forms was evaluated and compared to the data reported in the literature for natural oxalates.[29] On this basis, a linear law giving the phase transition temperature as a function of the chemical composition was determined.

Experimental Section

Synthesis. Chemical reagents were supplied by VWR, Merck, and Aldrich-Fluka. A concentrated thorium chloride solution ($C \approx 1.8$ M) was issued from Rhodia, while uranium chloride was obtained by dissolving uranium metal chips in 4 M hydrochloric acid. The initial solutions were then diluted, and final concentrations were estimated to be 0.7 and 1.1 M, respectively, using a titration method developed by Dacheux et al.[30−33] In order to check the uranium oxidation state in the final hydrochloric solution, several methods were used, including UV−visible spectroscopy (mainly focused in the 350−450 nm and 600−700 nm areas for U(VI) and U(IV), respectively), as already described when discussing the synthesis of thorium−uranium(IV) phosphates.[34] Additionally, the direct comparison of titration results obtained for total uranium (spectrophotometry after complete oxidation of uranium(IV) into uranyl by H_2O_2 in nitric acid) and uranium(IV) (back-titration by iron(II) sulfate) of the excess potassium dichromate resulting from the oxidation of U(IV) by the $Cr_2O_7^{2-}$ ion led us to conclude that less than 1% of global uranium was oxidized as UO_2^{2+} in the prepared solution.[31,34]

The synthesis of $Th_{1-x}U_x(C_2O_4)_2 \cdot 2H_2O$ solid solutions for $0 \le x \le 0.8$ started from the initial precipitation of a stoichiometric mixture of hydrochloric solutions containing the cations introduced in a PTFE container by the dropwise addition of a weak excess ($\approx 2\%$) of an oxalic acid solution ($C \approx 1.8$ M). The PTFE container was introduced in a closed 45 mL Parr acid digestion bomb, then heated in an oven for a week at 130 °C. The operating conditions in terms of heating time and temperature were fixed in order to obtain an optimal crystallization state of the samples, that is, the lower average FWHM values on XRD patterns. The precipitates obtained were separated from the supernatant by filtration or centrifugation, washed several times

(11) Matthews, R. B.; Davies, N. C. OSTI Technical Report, no. PNL-3210, Office of Scientific and Technical Information, U.S. Dept. of Energy, Oak Ridge, TN, **1979**.
(12) Hubert, S.; Barthelet, K.; Fourest, B.; Lagarde, G.; Dacheux, N.; Baglan, N. *J. Nucl. Mater.* **2001**, *297*, 206–213.
(13) Mitra, N. K.; Mahapatra, S. S.; Chattopadhyay, A. K. *J. Ind. Chem. Soc.* **1983**, *60*, 499–501.
(14) Ananthasivan, K.; Anthonysamy, S.; Singh, A.; Vasudeva Rao, P. R. *J. Nucl. Mater.* **2002**, *306*, 1–9.
(15) Pope, J. M.; Radford, K. C. *J. Nucl. Mater.* **1974**, *52*, 241–254.
(16) Duvieubourg-Garela, L.; Vigier, N.; Abraham, F.; Grandjean, S. *J. Solid State Chem.* **2008**, *181*, 1899–1908.
(17) Ziegelgruber, K. L.; Knope, K. E.; Frisch, M.; Cahill, C. L. *J. Solid State Chem.* **2008**, *181*, 373–381.
(18) Clavier, N.; Dacheux, N.; Wallez, G.; Quarton, M. *J. Nucl. Mater.* **2006**, *352*, 209–216.
(19) Baeva, E. E.; Mikhailov, Y. N.; Gorbunova, Y. E.; Serezhkina, L. B.; Serezhkin, V. N. *Russ. J. Inorg. Chem.* **2002**, *47*, 1348–1352.
(20) Baeva, E. E.; Mikhailov, Y. N.; Gorbunova, Y. E.; Serezhkina, L. B.; Serezhkin, V. N. *Russ. J. Inorg. Chem.* **2003**, *48*, 1651–1657.
(21) Chapelet-Arab, B.; Nowogrocki, G.; Abraham, F.; Grandjean, S. *Radiochim. Acta* **2005**, *93*, 279–285.
(22) Chapelet-Arab, B.; Nowogrocki, G.; Abraham, F.; Grandjean, S. *J. Solid State Chem.* **2005**, *178*, 3046–3054.
(23) Chapelet-Arab, B.; Nowogrocki, G.; Abraham, F.; Grandjean, S. *J. Solid State Chem.* **2005**, *178*, 3055–3065.
(24) Chapelet-Arab, B.; Duvieubourg, L.; Nowogrocki, G.; Abraham, F.; Grandjean, S. *J. Solid State Chem.* **2006**, *179*, 4029–4036.
(25) Chapelet-Arab, B.; Grandjean, S.; Nowogrocki, G.; Abraham, F. *J. Nucl. Mater.* **2008**, *373*, 259–268.
(26) Bressat, R.; Claudel, B.; Trambouze, Y. *J. Chem. Phys.* **1963**, *60*, 1265–1269.
(27) Jenkins, I. L.; Moore, F. H.; Waterman, M. J. *J. Inorg. Nucl. Chem.* **1965**, *27*, 81–87.
(28) Grigor'ev, M. S.; Charushnikova, I. A.; Krot, N. N. *Radiochemistry* **1997**, *35*, 419–422.
(29) Frost, R. L. *Anal. Chim. Acta* **2004**, *517*, 207–214.
(30) Dacheux, N.; Brandel, V.; Genet, M. *New J. Chem.* **1995**, *19*, 15–25.
(31) Dacheux, N.; Brandel, V.; Genet, M. *New J. Chem.* **1995**, *19*, 1029–1036.
(32) Brandel, V.; Dacheux, N.; Pichot, E.; Genet, M.; Emery, J.; Buzaré, J. Y.; Podor, R. *Chem. Mater.* **1998**, *10*, 345–350.
(33) Dacheux, N.; Podor, R.; Brandel, V.; Genet, M. *J. Nucl. Mater.* **1998**, *252*, 179–186.
(34) Dacheux, N.; Brandel, V.; Genet, M.; Bak, K.; Berthier, C. *New J. Chem.* **1996**, *20*, 301–310.

with deionized water and ethanol, dried at about 70 °C overnight, and then finally ground in an agate mortar.

Powder X-Ray Diffraction. After preparation of pure powdered samples for each studied composition (x = 0, 0.1, 0.3, 0.5, 0.6, 0.8), the unit cell parameters were refined by using powder X-ray diffraction data collected with a Bruker D8 θ/θ diffractometer equipped with Cu Kα radiation ($\lambda = 1.54178$ Å), using Bragg−Brentano geometry, with steps of 0.02° and a counting time of 20 s per step, within an angular range of 5−80° in 2θ. The unit cell parameters were refined from the powder diffraction pattern using the Rietveld method.[35,36] The refinement was carried out using the "*pattern matching*" option of the Fullprof program,[37] where only the profile parameters (cell dimensions, peak shapes, background, zero point correction, and symmetry) were refined. The peak shape was described by a pseudo-Voigt function with an asymmetry correction at low angles. In order to describe the angular dependence of the peak full-width at half-maximum (H), the formulation of Caglioti et al.[38] was used: $H^2 = U \tan^2 \theta + V \tan \theta + W$ where the U, V, and W parameters were refined in the process.

The high-temperature X-ray powder diffraction patterns were recorded using a BRUKER AXS D8 advance powder diffractometer (Cu Kα radiation) in θ/θ Bragg−Brentano geometry equipped with an HTK 1200 Anton Paar chamber and a PSD detector (Super Speed VANTEC-1). The samples were deposited on an alumina holder. Experiments were performed over a temperature range from room temperature to 120 °C in an air atmosphere. The high-temperature X-ray diagrams (HT-XRD) were recorded between 8 and 70° (2θ domain) with a step of 0.015° (2θ) and a counting time of 30 min per diagram.

Single-Crystal X-Ray Diffraction and Structure Determination. For the crystal structure determinations, well-shaped greenish single crystals of $Th_{1-x}U_x(C_2O_4)_2 \cdot 2H_2O$ solid solution, with $x = 0$, 0.5, and 1, were selected, mounted on fiberglass, and aligned on a Bruker X8 diffractometer equipped with an APEX II CCD detector. The X-ray intensity data were measured at room temperature using Mo Kα radiation (λ = 0.71073 Å) selected by a graphite monochromator. For each single crystal, a strategy based on a combination of Φ and Ω scans was chosen, with a rotation of 0.3° and an acquisition time of 30 s per frame. According to the cell parameters of each compound and the high quality of the selected crystals, the scan angles were adjusted to limit the overlapping of reflections. Thus, the diffracted intensities were collected up to 2θ = 83.22°, 81.42°, and 87.38° for $x = 0$, 0.5, and 1, respectively. After each data collection, intensities were reduced and corrected for Lorentz polarization and background effects using the SAINT 7.12 software.[39] Once the data processing was performed, the absorption corrections were computed using a semiempirical method based on redundancy using the SADABS 2004/1 program.[40]

Monoclinic unit cells were refined, leading to parameter unit cells with integrating independent reflections ($> 2\sigma(I)$). For each collection, examination of the systematic absences (hkl, $h + k = 2n + 1$ and $h0l$, $l = 2n + 1$) led to the choice of the $C2/c$ space group. The crystal structure was solved by direct methods using the XS program of the SHELXTL software package[41] that localizes the heavy atoms, that is, uranium or thorium. The oxygen, carbon, and hydrogen atomic positions were deduced from subsequent refinements and difference Fourier syntheses using the XL option of the SHELXTL software. The atomic scattering factors for neutral atoms were taken from the "International Tables for X-Ray Crystallography".[42] A twin model of monoclinic symmetry with $\beta \approx 90°$ (twining matrix [100, 0−10, 00−1] and refined ratio BASF = 0.47434, 0.52207, and 0.48393 for x = 0, 0.5 and 1, respectively) was used. Crystal data, conditions of data collection, and structure refinement parameters are reported in Table 1.

The single crystal of $Th_{0.5}U_{0.5}(C_2O_4)_2 \cdot 2H_2O$ was heated using an Oxford Cryosystems 700 heating device on a Bruker SMART diffractometer equipped with an APEX II CCD detector. The X-ray intensity data were measured at 90 °C using the same data collection, reduction, and correction procedures. The orthorhombic unit cell was refined, leading to a = 10.4843(3) Å, b = 8.5344(2) Å, and c = 9.5975(2) Å. The structure was solved in the *Ccca* space group.

Analysis. SEM micrographies were obtained with a Hitachi S-4800 high-resolution microscope or an FEI QUANTA FEG 200 ESEM environmental scanning electron microscope.

Electron probe microanalyses (EPMA) were carried out using a Cameca SX50 or SX100 apparatus. Adequate conditions of analysis were set at an acceleration voltage of 15 kV and 10 nA with counting times of 10 s on peak and 5 s on background. The electron beam was focused in order to perform the analysis on a 1−3 μm^3 volume. Thoria ThO_2 (M_α ray of thorium) and urania $UO_{2.12}$ (M_β ray of uranium) were used as calibration standards. For each sample, the average of at least 10 measurements was considered.

Spectroscopy. Finally, μ-Raman spectra were recorded with a Horiba-Jobin Yvon Aramis apparatus equipped with a Notch filter and using a He−Ne (632.8 nm) or a Nd:YAG (532 nm) laser. The laser beam was focused on the sample using an Olympus BX 41 microscope, resulting in a spot size of about 1 μm^2. In order to avoid any structural effect due to the laser beam, the power applied to the samples was set to 4 mW. At least four different locations were investigated at the surface of each sample, usually considering a dwell time of 10 s and an average of five scans.

In situ temperature measurements were undertaken thanks to a Linkam TS1500 hot stage cooled by a water flow. The sample was placed in a platinum crucible and heated from room temperature to 140 °C at a rate of 20 °C min^{-1}. Spectra were acquired every 3 °C considering a dwell time of 10 s and an average of at least three scans. In order to eliminate the eventual contribution of heterogeneities in the solid, one grain was followed during heating, and the repeatability of the measure was checked at several points in the sample.

Results and Discussion

1. $Th_{1-x}U_x(C_2O_4)_2 \cdot 2H_2O$ Solid Solutions. 1.1. SEM and EPMA Characterization. From SEM observations, the morphology of the powders was found to be strongly dependent on the chemical composition, that is, on the x substitution rate (Figure 1). For $x = 0$ (thorium oxalate), the sample is mainly constituted of well-defined small single crystals of 20−50 μm. When introducing tetravalent uranium in the solids, the shape of the grains stretches to give birth to bipyramidal crystals. Moreover, for the highest uranium contents, they appear to be less defined, while the apparition of a second population of small micrometric grains was observed in the samples during granulometric experiments.

(35) Rietveld, H. M. *Acta Crystallogr.* **1967**, *22*, 151–152.
(36) Rietveld, H. M. *Acta Crystallogr.* **1992**, *25*, 589–610.
(37) Rodriguez Carvajal, J.; Fernandez Diaz, M. T.; Martinez, J. L. *J. Phys.: Cond. Matter.* **1991**, *3*, 3215–3234.
(38) Caglioti, C.; Paoletti, A.; Ricci, E. P. *Nucl. Instr. Methods* **1958**, *3*, 223–228.
(39) *SAINT+*, version 7.12; Bruker Analytical X-ray Systems: Madison, WI, 2004.
(40) Sheldrick, G. M. *SADABS*, Bruker-Siemens Area Detector Absorption and Other Correction, Version 2004/1; Univeristy of Goetingen: Goetingen, Germany, 2004.
(41) Sheldrick, G. M.; *SHELXTL PC*, version 6.12; Siemens Analytical X-ray Instruments, Inc.: Madison, WI, 2001.
(42) *International Tables for X-Ray Crystallography*; Kynoch Press: Birmingham, AL, 1974; Vol. *IV*.

Table 1. Crystal Data, Intensity Collection, and Structure Refinement Parameters for α-$Th_{1-x}U_x(C_2O_4)_2 \cdot 2\ H_2O$, $x = 0$, 0.5, 1 and β-$Th_{0.5}U_{0.5}(C_2O_4)_2 \cdot 2\ H_2O$

	α-$Th(C_2O_4)_2 \cdot 2H_2O$	α-$Th_{0.5}U_{0.5}(C_2O_4)_2 \cdot 2H_2O$	α-$U(C_2O_4)_2 \cdot 2H_2O$	β-$Th_{0.5}U_{0.5}(C_2O_4)_2 \cdot 2H_2O$
		crystal data		
cryst symmetry	monoclinic	monoclinic	monoclinic	orthorhombic
space group	*C* 2/c (n° 15)	*C* 2/c	*C* 2/c	*Ccca* (n° 68)
chemical formula weight (g mol^{-1})	444.11	447.11	450.10	447.11
unit cell	*a* = 10.4029(7) Å *b* = 8.4756(6) Å *c* = 9.7566(6) Å β = 90.041(3)° *V* = 860.20(1) $Å^3$	*a* = 10.4020(5) Å *b* = 8.4631(4) Å *c* = 9.6787(4) Å β = 90.019(2)° *V* = 852.05(7) $Å^3$	*a* = 10.4213(7) Å *b* = 8.4586(6) Å *c* = 9.5290(7) Å β = 90.082(4)° *V* = 839.98(9) $Å^3$	*a* = 10.4843(3) Å *b* = 8.5344(2) *c* = 9.5975(2) *V* = 858.76(4) $Å^3$
Z	4	4	4	4
density (g/cm^3)	3.429(1)	3.485(1)	3.559(1)	3.457(2)
		data collection		
temperature (K)	296(2)	296(2)	296(2)	363(3)
radiation Mo(Kα)	0.71073 Å	0.71073 Å	0.71073 Å	0.71073 Å
scan mode	ω scans	ω scans	ω scans	φ and ω scans
recording angular range (deg)	2.09−41.61	2.10−40.71	2.14−43.69	3.74−43.30
recording reciprocal space	$-18 \le h \le 18$ $-15 \le k \le 13$ $-17 \le l \le 19$	$-17 \le h \le 19$ $-14 \le k \le 15$ $-17 \le l \le 17$	$-19 \le h \le 19$ $-15 \le k \le 15$ $-16 \le l \le 18$	$-13 \le h \le 20$ $-12 \le k \le 16$ $-18 \le l \le 16$
measured reflns	21904	22630	13323	13049
R equivalents: R_{int}	0.0249	0.0308	0.0309	0.0339
independent reflns	2779	2721	3129	1592
absorption μ (cm^{-1})	173.78	183.20	193.37	183.20
		refinement[a]		
refined params/restraints	79/0	79/0	78/0	40/0
goodness of fit on F^2	1.078	1.013	1.027	1.128
R1 [$I > 2\sigma(I)$]	0.017	0.013	0.017	0.021
wR2 [$I > 2\sigma(I)$]	0.035	0.027	0.032	0.041
R1 [all data]	0.026	0.018	0.028	0.043
wR2 [all data]	0.038	0.029	0.036	0.045
largest diff peak and hole (e $Å^{-3}$)	2.558/−1.192	1.522/−1.515	1.901/−2.710	1.126/−0.945

[a] $R1 = \sum(|F_o| - |F_c|)/\sum|F_o|$. $wR2 = [\sum w(F_o^2 - F_c^2)^2/\sum w(F_o^2)^2]^{1/2}$. $w = 1/[\sigma^2(F_o^2) + (aP)^2 + bP]$, where *a* and *b* are refinable parameters and $P = (F_o^2 + 2F_c^2)/3$.

EPMA experiments confirmed that all the compounds were single phase since the elementary weight loadings as well as the mole ratios agreed well with the calculated values (Table 2). Particularly, the uranium amount was found consistent with that expected which confirms that the oxidation state (+IV) was fully stabilized in the initial solution and during the crystallization step, leading to a quantitative precipitation.

1.2. Powder X-Ray Diffraction. The X-ray powder diffraction patterns of the samples prepared for $0 \le x \le 0.8$ are close to that previously reported for $M(C_2O_4)_2 \cdot 2H_2O$ (M = Th, U)[26,27] and indexed in an orthorhombic unit cell. However, splitting of some reflections indicates a less symmetric cell. In fact, all of the reflections can be indexed in a monoclinic unit cell (C-centered) with refined unit cell parameters close to those of the orthorhombic cell (Table 3). Figure 2 shows the good agreement between observed and calculated powder X-ray diffraction patters for $Th_{0.7}U_{0.3}(C_2O_4)_2 \cdot 2H_2O$, while the splitting of reflections is zoomed in the insets. Figure 3 shows a nearly linear variation of the unit cell parameters with *x*, confirming the existence of a solid solution. The *b* and *c* parameters which correspond to the two-dimensional actinide−oxalate arrangement slightly decrease when *x* increases. This trend is in agreement with the ionic radius decreasing from Th(IV) to U(IV). Meanwhile, the *a* parameter, which corresponds to the interlayer distance slightly increases. These results show that the monoclinic distortion of the unit cell diminishes from Th to U end members. Furthermore, the deterioration of the crystallinity with the uranium amount leads to an overlapping of the split reflections for $U(C_2O_4)_2 \cdot 2H_2O$: under these conditions, the monoclinic unit cell parameters are not well refined and do not fit with the variation throughout the solid solution.

1.3. Crystal Structure Determination of $Th_{1-x}U_x(C_2O_4)_2 \cdot 2H_2O$, $x = 0$, 0.5, 1. The crystal structure of the uranium(IV) oxalate dihydrate has been recently reported with orthorhombic symmetry using the *Ccca* space group.[16] Refinement of the unit cell parameters from the powder XRD pattern led to *a* = 8.5449(8) Å, *b* = 10.497(7) Å, and *c* = 9.419(8) Å, which was in agreement with previously reported results.[26,27] Moreover, a preliminary structural approach recently performed using a $Th(C_2O_4)_2 \cdot 2H_2O$ single crystal obtained with a hydrothermal reaction and in situ oxalate synthesis[17] suggested an orthorhombic unit cell with *a* = 8.4573(8) Å, *b* = 10.3764 (10) Å, and *c* = 9.7533(9) Å and a layered structure isotypic with that of $U(C_2O_4)_2 \cdot 2H_2O$.

Single crystals of $Th(C_2O_4)_2 \cdot 2H_2O$ and $Th_{0.5}U_{0.5}(C_2O_4)_2 \cdot 2H_2O$ were selected under an optical microscope for an X-ray crystal structure study. A first approach confirmed the orthorhombic unit cell and a structure isotypic with that of $U(C_2O_4)_2 \cdot 2H_2O$.[16] However, as in the uranium compound, the U_{11} atomic displacement parameter for the atom O(1) was too weak. Moreover,

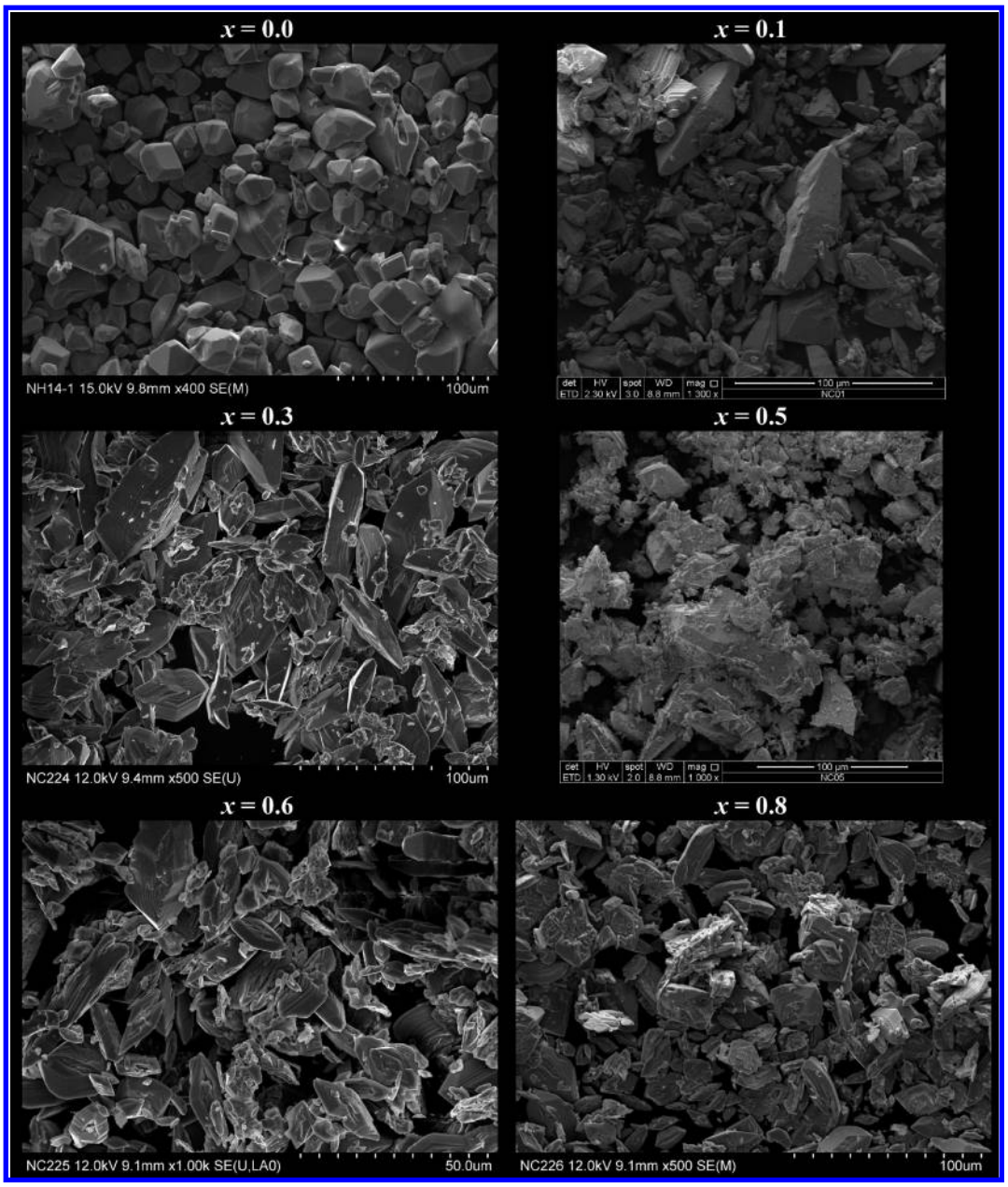

Figure 1. SEM micrographies of $Th_{1-x}U_x(C_2O_4)_2 \cdot 2H_2O$ solid solutions.

Table 2. EPMA Results for $Th_{1-x}U_x(C_2O_4)_2 \cdot 2H_2O$ Solid Solutions

	wt (%) Th		wt (%) U		U/(Th + U)
x substitution rate	calcd	exptl	calcd	exptl	exptl
0	52.3	52.4 ± 0.1			
0.1	47.0	48.8 ± 0.8	5.4	4.8 ± 0.8	0.09 ± 0.02
0.3	36.4	37.8 ± 1.7	16.0	15.6 ± 1.7	0.30 ± 0.03
0.5	26.0	27.4 ± 1.8	26.6	27.3 ± 1.6	0.50 ± 0.01
0.6	20.7	22.2 ± 2.1	31.9	33.7 ± 2.3	0.61 ± 0.04
0.8	10.3	12.0 ± 1.1	41.4	41.0 ± 1.0	0.78 ± 0.02

a close examination of the reciprocal space revealed a splitting of the reflexions, so the crystal structure was refined in a monoclinic cell in agreement with the powder results, and a twinning of the crystal was introduced (see the Experimental Section). The results were thus improved. All of the atomic displacement parameters have acceptable values, and even the hydrogen atoms of the water molecules were located and their coordinates

Table 3. Refined Unit Cell Parameters and Volume of $Th_{1-x}U_x(C_2O_4)_2 \cdot 2\ H_2O$ Solid Solutions and Comparison with Re-examined $U(C_2O_4)_2 \cdot 2H_2O$

x	*a* (Å)	*b* (Å)	*c* (Å)	*β* (°)	V (Å^3)
0.0	10.3881(3)	8.4641(3)	9.7508(4)	90.497(3)	857.3(1)
0.1	10.3938(2)	8.4633(2)	9.7401(2)	90.470(2)	856.8(1)
0.3	10.3951(2)	8.4616(2)	9.7044(2)	90.449(1)	853.6(1)
0.5	10.3994(3)	8.4611(3)	9.6719(3)	90.430(2)	851.0(1)
0.6	10.4054(3)	8.4603(2)	9.6403(3)	90.403(2)	848.6(1)
0.8	10.4135(2)	8.4558(2)	9.5799(2)	90.361(1)	843.5(1)
1.0	10.4552(9)	8.5071(8)	9.4208(8)	90.322 (7)	837.9(3)

refined. The crystal structure of $U(C_2O_4)_2 \cdot 2H_2O$ was thus re-examined in the monoclinic symmetry using a single crystal prepared as described by Duvieubourg-Garela et al.,[16] and this confirmed the results obtained for the thorium-bearing compounds.

The main features of the structure previously described in the orthorhombic symmetry for the uranium compound are confirmed: the structure is built from a

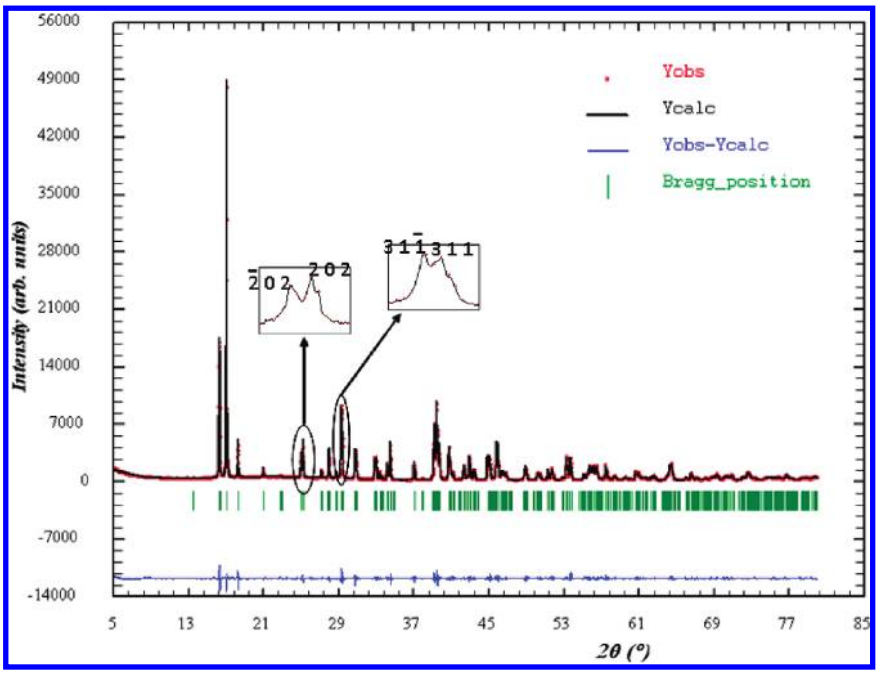

Figure 2. Observed (Y_{obs}), calculated (Y_{cal}), and difference profiles ($Y_{obs} - Y_{cal}$) from refinement of X-ray powder diffraction data of $Th_{0.7}U_{0.3}(C_2O_4)_2 \cdot 2H_2O$. Allowed reflections are indicated by vertical lines. The splitting of some reflections corresponding to the orthorhombic to monoclinic symmetry change is shown in the insets.

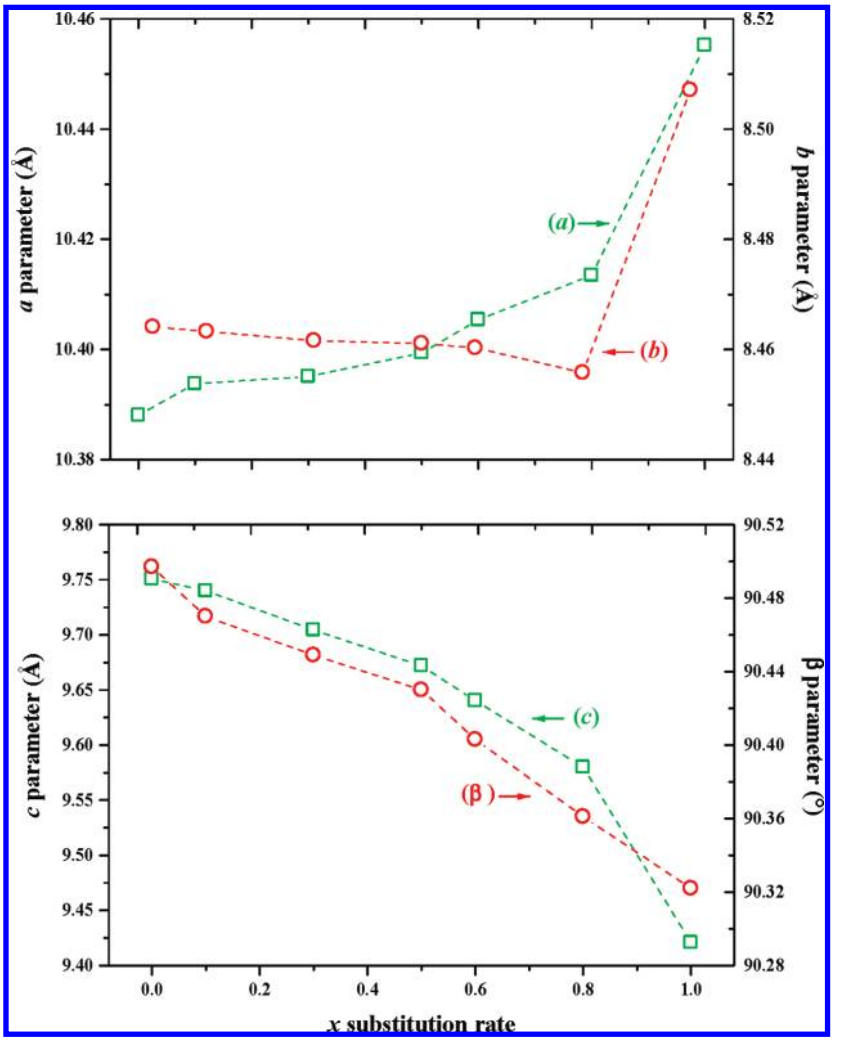

Figure 3. Variation of the unit cell parameters of $Th_{1-x}U_x(C_2O_4)_2 \cdot 2H_2O$ solid solutions versus substitution rate x.

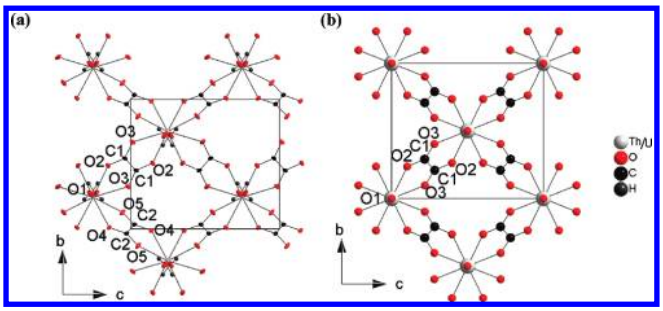

Figure 4. Projection along the *a* axis of the metal organic framework of $Th_{1-x}U_x(C_2O_4)_2\cdot 2H_2O$ at room temperature (α form) (a) and above the transition (*β* form) (b).

Table 4. Main Interatomic Distances (Å) for α-$Th_{1-x}U_x(C_2O_4)_2\cdot 2H_2O$, x = 0, 0.5, 1 and *β*-$Th_{0.5}U_{0.5}(C_2O_4)_2\cdot 2H_2O$

	RT			90 °C
	d_{Th-O}	$d_{Th/\underline{U}-O}$	$d_{\underline{U}-O}$	$d_{Th/\underline{U}-O}$
M−O2 (2 ×)	2.480(2)	2.460(2)	2.433(3)	(4 ×) 2.462(2)
M−O4 (2 ×)	2.482(2)	2.469(2)	2.452(3)	
M−O5 (2 ×)	2.508(4)	2.493(3)	2.452(7)	
M−O1 (2 ×)	2.512(2)	2.498(2)	2.483(2)	(2 ×) 2.517(3)
M−O3 (2 ×)	2.551(3)	2.541(2)	2.500(6)	(4 ×) 2.501(2)
average	2.507(2)	2.492(2)	2.464(4)	2.490(2)
		d_{C-O}		
C1−O3	1.242(3)	1.243(2)	1.241(3)	1.233(4)
C1−O2	1.255(4)	1.255(3)	1.254(4)	1.259(3)
C2−O5	1.240(4)	1.238(3)	1.244(4)	
C2−O4	1.261(4)	1.263(3)	1.244(4)	
		d_{C-C}		
C1−C1	1.523(4))	1.529(3)	1.525(6)	1.530(4)
C2−C2	1.546(4))	1.545(3)	1.538(5)	
		d_{H-O}		
O1−H1	0.89(6))	0.85(4)	0.91(5)	0.83(6)
O1−H2	0.85(6)	0.77(6)	0.60(7)	

two-dimensional metal organic framework parallel to the (1 0 0) plane resulting from M(IV) (M = U, Th) centers connected trough bis-bidentate oxalate ions (Figure 4a); the metallic atom is coordinated by eight oxygen atoms from four oxalate entities and two water oxygen atoms forming a bicapped (by oxygen coming from water) square antiprism (Table 4). The layers are stacked in the [1 0 0] direction in an ABAB fashion; two adjacent layers are translated so that the metals of one layer are above the center of the square of the metal-oxalate four-side cycle of the adjacent layers. However, in the actual monoclinic symmetry, the unit cell contains two independent oxalate ions, $(C1O2O3)_2$ and $(C2O4O5)_2$, both possessing a symmetry center at the middle of the C−C bond. The precise location of hydrogen atoms allows us to propose a hydrogen bond scheme between the layers (Figure 5a): one water oxygen is connected to two oxalates that belong to the environment of the same metal of the adjacent layer through a short hydrogen bond involving the H1 atom to the O(4) atom of one oxalate moiety and through a bifid hydrogen bond involving H2 to two oxygen atoms, O(2) and O(3), belonging to the same carboxylate part of another oxalate ion (Table 5).

1.4. *μ*-Raman Investigations. The *μ*-Raman spectra recorded for $Th(C_2O_4)_2\cdot 2H_2O$ (Figure 6) and $Th_{1-x}U_x(C_2O_4)_2\cdot 2H_2O$ solid solutions are in good agreement with the rich literature devoted to natural oxalates.[29,43−49] Below 300 cm^{-1}, the numerous vibration bands observed correspond to the elongation and the deformation of the An^{IV}−O bonds, as well as to the lattice modes. The doublet observed near 500 and 520 cm^{-1}, as well as the band close to 790 cm^{-1}, was assigned to the δ(O−C−O) bending and rocking modes, while the stretching of the C−C bond was correlated to the band recorded at around 920 cm^{-1}. Above 1000 cm^{-1}, the two bands observed at 1480 cm^{-1}, on the one hand, and at 1630 cm^{-1}, on the other hand, were linked to the symmetric (ν_s) and antisymmetric (ν_{as}) stretching modes of the C−O vibration, respectively.

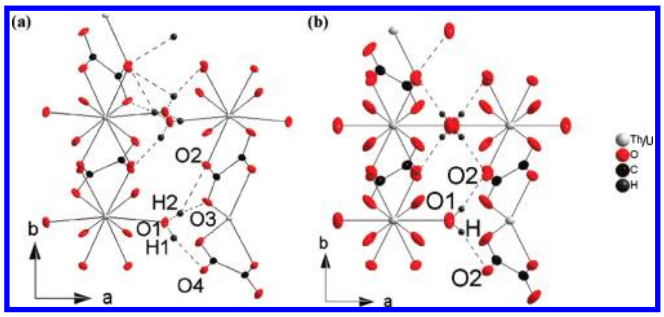

Figure 5. Scheme of hydrogen bonding between the layers for the α form (a) and the *β* form (b) of $Th_{1-x}U_x(C_2O_4)_2\cdot 2H_2O$.

It is worth noting the existence of a doublet for the ν_s(C−O) vibration mode, in good agreement with the XRD study which allowed for the pointing out of two distinct oxalate ions in the unit cell. Indeed, the group theory assignment under the C_i symmetry theoretically only allows one vibration mode (A_g) for the ν_s(C−O) stretching,[50,51] and the double band observed probably came from this structural feature. Also, even if the presence of two bands in the 1450−1490 cm^{-1} region has been already described in the literature, no satisfying explanation was proposed. Among them, Ito et al. assigned the 1450 cm^{-1} band to the combination $\nu_5 + \nu_9$,[52] while Begun argued for a resonance band corresponding to $2\nu_8$,[53] but both authors were contradicted.[54] Another argument lies in the possible presence of free oxalates in the system, which can be responsible for the additional band.[55,56] Nevertheless, it appears to be widely unlikely in our study, even if some oxalates could remain adsorbed at the surface of the solids despite the washing steps

(43) Shippey, T. A. *J. Mol. Struct.* **1980**, *63*, 157–166.
(44) Edwards, H. G. M.; Russell, N. C.; Seaward, M. R. D. *Spectrochim. Acta A* **1997**, *53*, 99–105.
(45) Frost, R. L.; Weier, M. L. *J. Raman Spectrosc.* **2003**, *34*, 776–785.
(46) Frost, R. L.; Weier, M. L. *Thermochim. Acta* **2003**, *406*, 221–232.
(47) Frost, R. L. *Spectrochim. Acta A* **2003**, *59*, 1195–1204.
(48) Frost, R. L.; Adebajo, M.; Weier, M. L. *Spectrochim. Acta A* **2004**, *60*, 643–651.
(49) D'Antonio, M. C.; Palacios, D.; Coggiola, L.; Baran, E. J. *Spectrochim. Acta A* **2007**, *68*, 424–426.
(50) Thomas, Y.; Six, P.; Chauvet, G.; Taravel, B.; Lorenzelli, V. *Physica* **1979**, *98C*, 131–139.
(51) Clark, R. J. H.; Firth, S. *Spectrochim. Acta A* **2002**, *58*, 1731–1746.
(52) Ito, K.; Bernstein, H. J. *Can. J. Chem.* **1956**, *34*, 170–178.
(53) Begun, G. M.; Fletcher, W. H. *Spectrochim. Acta* **1963**, *19*, 1343–1349.
(54) Shippey, T. A. *J. Mol. Struct.* **1980**, *65*, 61–70.
(55) Gruen, E. C.; Plane, R. A. *Inorg. Chem.* **1967**, *6*, 1123–1127.
(56) Hind, A. R.; Bhargava, S. K.; Van Bronswijk, W.; Grocott, S. C.; Eyer, S. L. *App. Spectrosc.* **1998**, *52*, 683–691.

Table 5. Hydrogen Bond Characteristics for α-$Th_{1-x}U_x(C_2O_4)_2\cdot 2H_2O$, $x = 0$, 0.5, 1 and β-$Th_{0.5}U_{0.5}(C_2O_4)_2\cdot 2H_2O$

	O1 − H1	H1···O4	O1···O4	O1−H1···O4	O1−H	H···O2	O1···O2	O1−H···O2
α-Th	0.89(4)	2.00(4)	2.870(5)	164(4)				
α-Th/U	0.85(4)	2.04(4)	2.881(3)	170(4)				
α-U	0.88(5)	2.02(5)	2.923(6)	172(5)				
β-Th/U					0.83(6)	2.19(6)	3.001(3)	165(5)

	O1−H2	H2···O3	O1···O3	O1−H2···O3	H2···O2	O1···O2	O1−H2···O2
α-Th	0.85(9)	2.37(9)	3.134(7)	150(7)	2.34(7)	3.083(4)	146(6)
α-Th/U	0.77(7)	2.42(7)	3.119(5)	151(7)	2.39(6)	3.086(3)	151(6)
α-U	0.60(7)	2.51(7)	3.09(1)	163(8)	2.60(7)	3.099(5)	143(8)

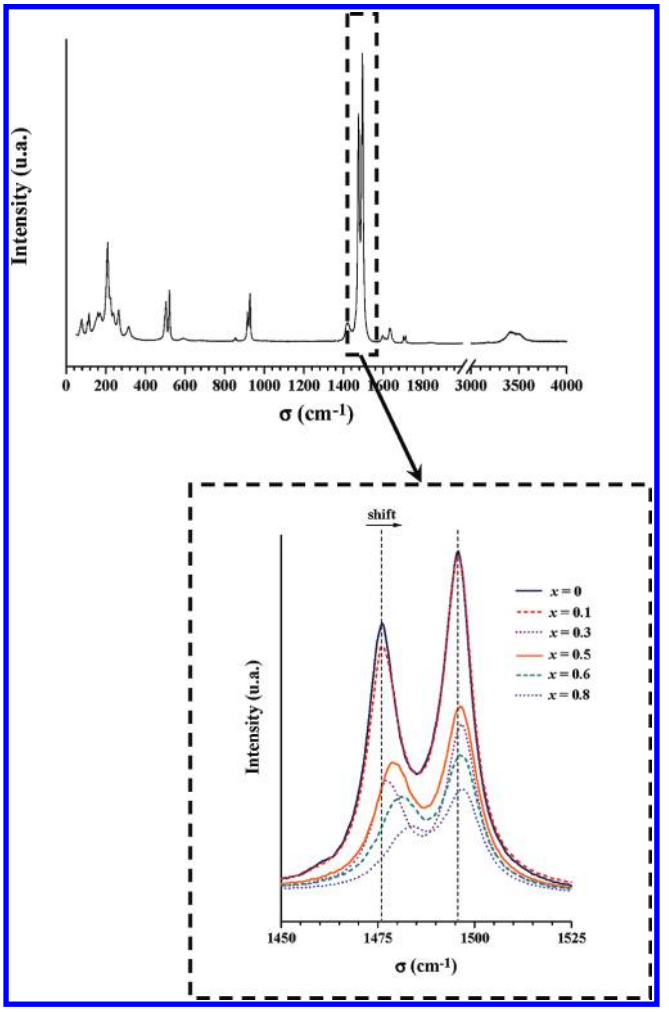

Figure 6. μ-Raman spectra of $Th(C_2O_4)_2\cdot 2H_2O$ and variation of the ν_s(C−O) doublet of $Th_{1-x}U_x(C_2O_4)_2\cdot 2H_2O$ solid solutions versus substitution rate x.

performed. Under these conditions, the ν_s(C−O) doublet could be correlated to original arrangement of the oxalate entities in the monoclinic structure.

Finally, the weak doublet observed at around 1705 cm^{-1} was assigned to the antisymmetric stretching vibration of the C−O bond in the presence of water, as was already described for several oxalate complexes.[57,58] Moreover, the presence of a doublet could corroborate the existence of two types of hydrogen bonds in the solid, as evidenced from the structural description. Although several bands remain unassigned, it could be assumed that they result from the interaction of the oxalate bonds with the water molecules. It could also be correlated to the combination of several vibrations, such as for the weak band observed at 1420 cm^{-1}, usually assigned to $(\nu_2 + \nu_3)$.[51]

Complementary IR experiments confirm the presence of the characteristic vibration modes of the oxalate species, particularly at around 1305−1350 cm^{-1} and 1605 cm^{-1} concerning the symmetric and antisymmetric stretching modes of the C−O bond, respectively.

The influence of the incorporation of uranium in the structure of $Th(C_2O_4)_2\cdot 2H_2O$ on the μ-Raman spectrum was also evaluated through the variation of the doublet corresponding to the ν_s(C−O) stretching mode emphasized in Figure 6. The spectrum of the thorium oxalate dihydrate was found to be slightly affected by the Th−U(IV) substitution since several bands appeared to be metal-sensitive, such as the δ(O−C−O) and ν(C−C) modes located around 520 cm^{-1} and 915 cm^{-1}, respectively. Among them, the ν_s(C−O) doublet appears particularly remarkable since the position of the second band remains unchanged during the substitution of thorium by uranium(IV), while the first one is shifted to the upper wavenumbers when x increases. Indeed, its position lies from 1476 to 1484 cm^{-1} between $x = 0$ and $x = 0.8$. These observations agree well with that reported by Morris and Hobart during the study of lanthanide oxalates.[59] Only the δ(O−C−O), ν(C−C), and ν_s(C−O) modes were found to be affected by the variation in the ionic radius along the series of rare earth elements. Among these vibrations, ν_s(C−O) appears as the most lanthanide-sensitive since its position varies between 1476 and 1499 cm^{-1} from lanthanum to erbium. In this study, the variation appears less important, due to the low difference in the ionic radius of thorium and uranium(IV).[60] Nevertheless, the ν_s(C−O) doublet remains the most affected and can be used as an original hint in the evaluation of the chemical composition of $Th_{1-x}U_x(C_2O_4)_2\cdot 2H_2O$ solid solutions.

In comparison, the IR spectrum of $Th(C_2O_4)_2\cdot 2H_2O$ seems to be less affected by the thorium−uranium(IV) substitution. The wide band assigned to the ν_{as}(C−O) vibration appeared to be split into two components for the thorium-based sample, while the two contributions became convoluted for mixed compounds. This tendency confirms the sensitivity of the C−O bond vibrations to the cationic environment, as evidenced from the μ-Raman

(57) Jaber, M.; Bertin, F.; Forel, M. T. *Can. J. Chem.* **1979**, *57*, 876–882.
(58) Hug, S.; Sulzberger, B. *Langmuir* **1994**, *10*, 3587–3597.
(59) Morris, D. E.; Hobart, D. E. *J. Raman Spectrosc.* **1988**, *19*, 231–237.
(60) Shannon, R. D. *Acta Crystallogr.* **1976**, *32*, 751–767.

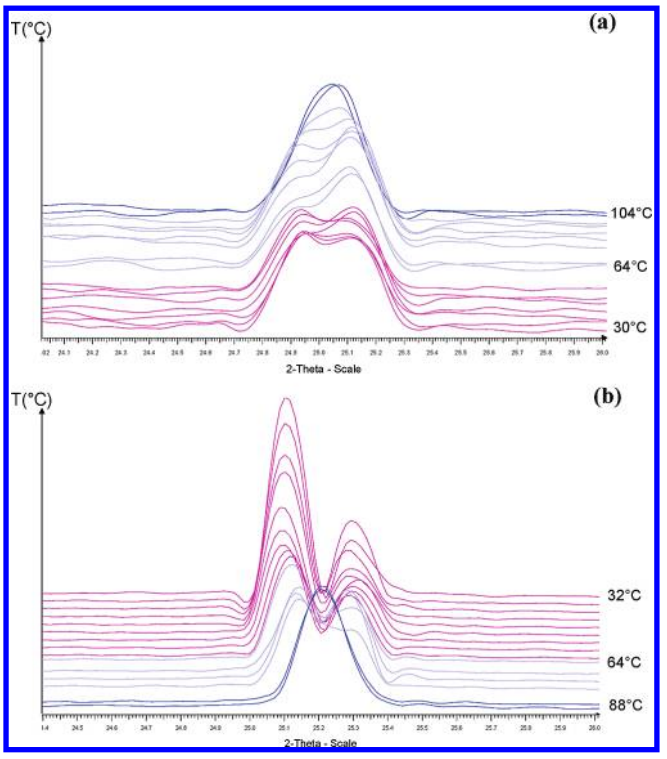

Figure 7. Variations of the (−2 0 2) and (2 0 2) reflections versus temperature during heating (a) and cooling (b) steps.

spectra. Nevertheless, it was hardly possible to follow the shift of the absorption bands with the variation of the chemical composition, and the IR spectroscopy then appears less efficient to evidence the influence of the uranium rate in the solid.

2. Phase Transformation. 2.1. Powder X-Ray Diffraction. The pseudo-orthorhombic unit cell at room temperature with systematically twinned monoclinic single crystals suggests a transition to an orthorhombic polymorph on heating. Thus, the X-ray diffraction doublet at about 25° in 2θ corresponding to (−2 0 2) and (2 0 2) reflections was recorded every 2 °C on heating for $Th(C_2O_4)_2 \cdot 2H_2O$ (Figure 7a). At about 64 °C, the relative intensity of the two reflections is reversed, while at 104 °C, they are transformed into only one peak. During the recording of the full pattern at 110 °C, with the goal of refinement of the orthorhombic unit cell parameters, the thorium oxalate undergoes a transformation into the monohydrate, and the reflection at about 25° in 2θ disappears. In fact, the dihydrate−monohydrate transformation temperature was reported to lie between 130 and 220 °C.[61−64] The same experiment was then realized on $Th_{0.5}U_{0.5}(C_2O_4)_2 \cdot 2H_2O$, for which monoclinic−orthorhombic transition is observed at a lower temperature (about 85 °C). The X-ray pattern collected at 92 °C allowed the refinement of the orthorhombic unit cell parameters to $a =$ 10.4898(3) Å, $b = 8.5366(4)$ Å, $c = 9.5945(3)$ Å (Figure 8). On cooling, the orthorhombic (denoted β form) to monoclinic (denoted α form) reverse transition occurs at 86 °C

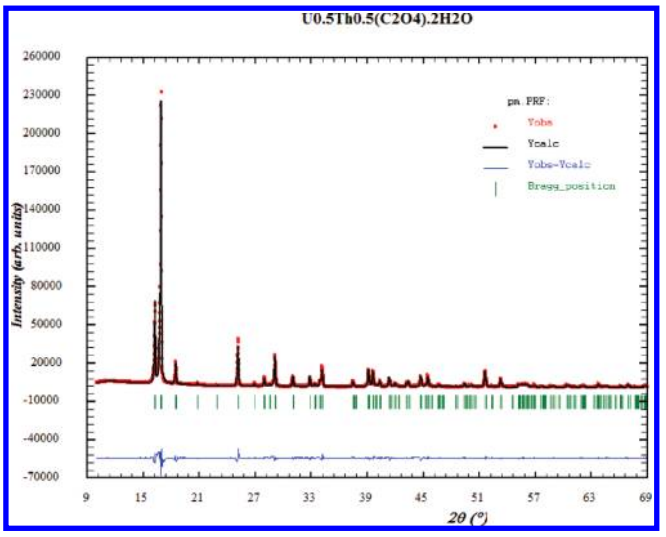

Figure 8. Observed (Y_{obs}), calculated (Y_{cal}), and difference profiles ($Y_{obs} - Y_{cal}$) from refinement of X-ray powder diffraction data of β-$Th_{0.5}U_{0.5}(C_2O_4)_2 \cdot 2H_2O$. Allowed reflections are indicated by vertical lines.

and is accompanied by the splitting of the (2 0 2) orthorhombic reflection (Figure 7b).

2.2. Crystal Structure Determination of $Th_{0.5}U_{0.5}(C_2O_4)_2 \cdot 2H_2O$. As previously observed from the powder X-ray diffraction experiments, for $Th(C_2O_4)_2 \cdot 2H_2O$, the orthorhombic phase dehydrates rapidly and the crystal is destroyed on heating at 110 °C. For $U(C_2O_4)_2 \cdot 2H_2O$, the single crystal is of lesser quality; furthermore, the transition temperature is too close to the room temperature (see section 2.3), so the measurement temperature is difficult to stabilize. Consequently, the intensities were collected at 90 °C using a $Th_{0.5}U_{0.5}(C_2O_4)_2 \cdot 2H_2O$ single crystal for the crystal structure determination of the orthorhombic phase. Conversely to the refinement at room temperature in the orthorhombic symmetry performed in a first stage, all of the displacement parameters have acceptable values. The main features of the structural arrangement are of course maintained. The major differences concern the symmetry of the uranium environment, which increases from *C*2 to *D*2 during the α to β transition. That leads to a linear Ow−U−Ow entity and to a unique oxalate ion (C1O1O2)$_2$ (Figure 4b). The oxygen−oxygen distances indicate that hydrogen bonds are built. They involve a water molecule and oxygen atoms O2 belonging to two different oxalate ions of the neighboring layer, leading to two equivalent bonds (Figure 5b) with Ow−O2 distances equal to 3.001(3) Å and a O2−Ow−O2 angle of 110.17(8)°. In fact, the last difference Fourier synthesis revealed a hydrogen atom near the Ow−O2 bond, which was introduced in the last refinement.

2.3. μ-Raman Investigations. In order to evaluate the consequences of the α → β phase transition of the thorium−uranium(IV) oxalate dihydrate on the μ-Raman spectra recorded from room temperature to 120 °C, in situ experiments were undertaken for several compositions of α-$Th_{1-x}U_x(C_2O_4)_2 \cdot 2H_2O$ solid solutions ($0 \leq x \leq 0.8$). Among all of the bands assigned to the characteristic vibrations of the oxalate group in the previous section, few of them seem to be affected by the heat treatment. The M−O and the lattice mode vibrations

(61) Aybers, M. T. *J. Nucl. Mater.* **1998**, *252*, 28–33.
(62) Joseph, K.; Sridharan, R.; Gnanasekaran, T. *J. Nucl. Mater.* **2000**, *281*, 129–139.
(63) Oktay, E.; Yayli, A. *J. Nucl. Mater.* **2001**, *288*, 76–82.
(64) Dash, S.; Krishnan, R.; Kamruddin, M.; Tyagi, A. K.; Raj, B. *J. Nucl. Mater.* **2001**, *295*, 281–289.

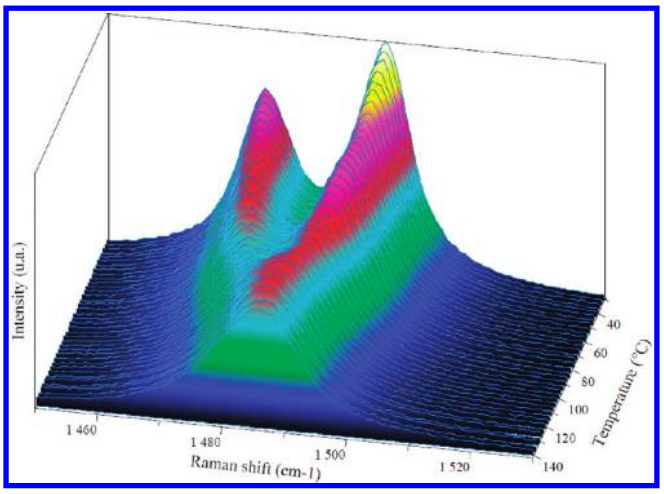

Figure 9. Variation of the ν_s(C−O) vibration band of $Th_{0.9}U_{0.1}(C_2O_4)_2\cdot 2H_2O$ versus heating temperature.

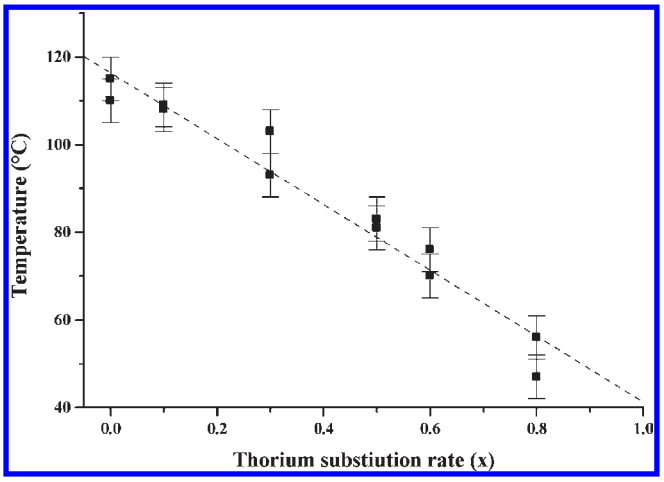

Figure 10. Variation of the α → β temperature transition of the $Th_{1-x}U_x(C_2O_4)_2\cdot 2H_2O$ solid solution versus x estimated from the μ-Raman spectra.

are slightly shifted to the lower wavenumbers (of about 5 cm^{-1}) as well as the δ(C−O) band around 305 cm^{-1}. Also, for the bands located at about 920 cm^{-1} (ν(C−C)), 1480 cm^{-1} (ν_s(C−O)), and 1705 cm^{-1} (ν_{as}(CO−H)), the doublet observed at room temperature progressively turned into a single band when increasing the temperature. This appears in good agreement with the structures determined from XRD data since the higher symmetry of the unit cell observed after the α→β phase transition led a unique oxalate group. Also, only one type of hydrogen bond could be achieved with the water molecules located between the layers. Under these conditions, the number of possible vibration modes corresponding to the C−C, the C−O···H, and the C−O bonds decreased, and the associated bands turned single along with the phase transformation. One can note that those vibrations were also among the most affected by the thorium substitution, which indicates a strong sensitivity to the structure, that is, to the oxalate group configuration. As for the cationic substitution, the most important modification of the spectrum lies in the progressive transformation of the ν_s(C−O) doublet (Figure 9). Under these conditions, the apparition of a single band at around 1490 cm^{-1} could be correlated with the phase transition and could be used to evaluate the temperature of transformation. From all of the spectra recorded from $Th_{1-x}U_x(C_2O_4)_2\cdot 2H_2O$ solid solutions between room temperature and 140 °C, the transition temperature appears to vary linearly with the uranium rate in the solid (Figure 10), while those determined for $x = 0$ and $x = 0.5$ are in very good agreement with the values obtained from HT-XRD experiments. The linear variation law deduced from the μ-Raman data also led to an evaluation of the temperature of transformation of pure uranium(IV) oxalate dihydrate at around 40 °C.

Conclusion

A complete $Th_{1-x}U_x(C_2O_4)_2\cdot 2H_2O$ solid solution was prepared for $0 \le x \le 1$ under mild hydrothermal conditions (T = 130 °C, t = 7 days) from a mixture of hydrochloric solutions containing cations and oxalic acid. A distortion of the previously reported orthorhombic cell to a monoclinic lattice has been evidenced throughout the solid solution, and a phase transition was evidenced through high-temperature XRD and μ-Raman studies.

The crystal structure of the low-temperature α form was determined in the monoclinic symmetry using twinned single crystals. It consists of a two-dimensional metal organic framework parallel to the (1 0 0) plane resulting from metallic centers connected trough bis-bidentate oxalate ions, the layers being stacked in the [1 0 0] direction in an ABAB fashion. In this monoclinic symmetry, the unit cell contains two independent oxalate ions, which results in the apparition of a doublet assigned to the ν_s(C−O) vibration in the μ-Raman spectra. This band was found to be very sensitive to the cationic environment and was proposed as an original hint in the estimation of the chemical composition of the samples. Finally, the accurate location of hydrogen atoms led us to determine the bonding scheme between the layers which featured one simple and one bifid hydrogen bond.

Following of the X-ray powder diffraction diagrams and μ-Raman spectra versus temperature then indicates a fully reversible transition to an orthorhombic β form at temperature varying from about 40 °C (uranium(IV) oxalate) to 110 °C (thorium oxalate). The crystal structure of the β form was determined at 90 °C for $Th_{0.5}U_{0.5}(C_2O_4)_2\cdot 2H_2O$ and mainly differs from the α form in the symmetry of the uranium environment, which increases from $C2$ to $D2$. This symmetrization led to a unique oxalate ion as well as to two equivalent hydrogen bonds linking the layers together. Under these conditions, the number of bands corresponding to the C−C, the C−O···H, and the C−O vibration modes observed in the μ-Raman spectra decreased. Particularly, the main modification of the spectrum lied in the progressive transformation of the ν_s(C−O) doublet during heat treatment. The apparition of a single band at around 1490 cm^{-1} was thus correlated to the phase transition and allowed the evaluation of the temperature of transformation of $Th_{1-x}U_x(C_2O_4)_2\cdot 2H_2O$ solid solutions. On this basis, the transition temperature was found to decrease linearly with the uranium amount in the solid, and a variation law was determined.

Several studies are now in progress to point out the partial dehydration of the $Th_{1-x}U_x(C_2O_4)_2\cdot 2H_2O$ solid solutions leading to thorium−uranium(IV) oxalate monohydrates and to determine accurately the crystal structure of the latter.

Acknowledgment. The authors would like to thank Alain Kohler and Johan Ravaux from the SCM of the University Nancy-I for SEM micrographs and EPMA experiments. This work was financially supported by the MATINEX Research Group (CEA/CNRS/AREVA/EDF/French Universities) included in the PACEN program. It also benefited from financial support of Agence Nationale de la Recherche (ANR-08-BLAN-0216).

Supporting Information Available: Crystallographic data in CIF file format, XRD diagrams and IR spectra of $Th_{1-x}U_x(C_2O_4)_2 \cdot 2H_2O$ solid solutions as well as complete assignment of IR and μ-Raman vibration bands. These materials are available free of charge via the Internet at http://pubs.acs.org.